Matthias Kogler and Berthold Stöger*

Hydrogen-bonding in mono-, di- and tetramethylammonium dihydrogenphosphites

https://doi.org/10.1515/zkri-2020-0088
Received October 14, 2020; accepted November 30, 2020;
published online January 18, 2021

Abstract: The crystal structures of methylammonium and dimethylammonium dihydrogenphosphite ($MA{\cdot}H_2PO_3$, $I2/a$ and $DMA{\cdot}H_2PO_3$, $P2_1/c$) are built of infinite chains of hydrogen bonded $H_2PO_3^-$ anions. The chains are connected by the ammonium cations via hydrogen bonding to di- ($DMA{\cdot}H_2PO_3$) and triperiodic ($MA{\cdot}H_2PO_3$) networks. Tetramethylammonium dihydrogenphosphite monohydrate ($TMA{\cdot}H_2PO_3{\cdot}H_2O$) features temperature dependent dimorphism. The crystal structure of the high-temperature (HT, cubic $P2_13$) and low-temperature (LT, orthorhombic $P2_12_12_1$) phases were determined at 150 and 100 K, respectively. The hydrogen bonding network in the HT phase is disordered, with $H_2PO_3^-$ and H_2O being located on a threefold axis and is ordered in the LT phase. On cooling, the point symmetry is reduced by an index of 3. The lost symmetry is retained as twin operations, leading to threefold twinning by pseudo-merohedry. The hydrogen-bonding networks of the HT and LT phases can be represented by undirected and directed quotient graphs, respectively.

Keywords: hydrogen bonding; phase transition; symmetry relations; twinning; voltage graphs.

1 Introduction

In our current line of research, we synthesized the 1:1 mono-, di-, tri- and tetramethylammonium salts of phosphorous acid $H_3P^{III}O_3$ as precursors to fluorine containing P^{III} compounds in reactions of the type

$$M H_2PO_3 + 5HF \rightarrow M HPF_5 + 3H_2O \quad (1)$$

where M stands for a monovalent cation. The nonhydrous mono- and dimethylammonium (MA and DMA) salts crystallized at 280 and 255 K, respectively. In contrast, the trimethylammonium salt remained an oil even at 255 K. The tetramethylammonium (TMA) salt, on the other hand, crystallized at 280 K with one molecule of crystal water, which was introduced by the $TMAOH{\cdot}5H_2O$ reactant.

As a routine analysis method, we determined the crystal structures of the crystalline salts at 100 K. In contrast to $MA{\cdot}H_2PO_3$ and $DMA{\cdot}H_2PO_3$, whose structures were trivially solved and refined, crystals of $TMA{\cdot}H_2PO_3{\cdot}H_2O$ were threefold twins of orthorhombic individuals with a pseudo-cubic symmetry. Since the crystals were optically isotropic at room temperature, we likewise determined their structure at higher temperatures. Indeed, at 150 and 200 K the crystals adopt a cubic symmetry.

The phase transition between the orthorhombic low-temperature (LT) and cubic high-temperature (HT) phases is due to the ordering of the hydrogen bonding network on cooling. Ordering of hydrogen bonding is one of the most important causes of order-disorder phase transitions in the solid state, the most well studied example probably being the potassium dihydrogen phosphate family of compounds [1]. The members of this family are ferroelectric below and paraelectric above the phase transition temperature.

In this work we present the order-disorder phase transition of $TMA{\cdot}H_2PO_3{\cdot}H_2O$. It will be analyzed in the light of symmetry reduction and the topology of the hydrogen bonding network. Moreover, the hydrogen bonding networks $MA{\cdot}H_2PO_3$ and $DMA{\cdot}H_2PO_3$ are discussed briefly.

2 Experimental

2.1 Synthesis and crystal growth

2.1.1 $MA{\cdot}H_2PO_3$: 3.53 g (38 mmol) $33\%_{wt}$ ethanolic $MeNH_2$ were added to 3.02 g (37 mmol) H_3PO_3 with stirring. The immediately precipitated white powder redissolved owing to heat of reaction. On cooling to 280 K, crystals of $MA{\cdot}H_2PO_3$ formed. The sample was single-phase according to X-ray powder diffraction (XRPD).

2.1.2 $DMA{\cdot}H_2PO_3$: 4.26 g (38 mmol) $40\%_{wt}$ aqueous Me_2NH was added to 3.01 g (37 mmol) H_3PO_3 with stirring. The solution was dried one day *in vacuo* over H_2SO_4. The residue crystallized at 255 K. Phase purity

***Corresponding author: Berthold Stöger**, X-Ray Centre, TU Wien, Getreidemarkt 9, 1060 Vienna, Austria,
E-mail: bstoeger@mail.tuwien.ac.at
Matthias Kogler, X-Ray Centre, TU Wien, Getreidemarkt 9, 1060 Vienna, Austria

could not be established using standard XRPD procedures owing to the deliquescence of the sample.

2.1.3 $Me_3NH{\cdot}H_2PO_3$: 6.19 g (37 mmol) $35\%_{wt}$ ethanolic Me_3N was added to 3.07 g (37 mmol) H_3PO_3 with stirring. The solution was immediately attached to a vacuum pump (10^{-4} mbar) for two days. The resulting viscous liquid did not crystallize even at 255 K for a prolonged time. Cooling using liquid N_2 led to formation of a glass, which melted when warming to 255 K. Analogous reaction from aqueous Me_3N and drying for two days at 10^{-4} mbar likewise afforded an oil, which didn't crystallize at 255 K. Likewise, drying in a vacuum desiccator over KOH followed by cooling did not result in crystallization.

2.1.4 $TMA{\cdot}H_2PO_3{\cdot}H_2O$: 3.09 g (37 mmol) H_3PO_3 and 6.64 g (37 mmol) $TMAOH{\cdot}5H_2O$ were dissolved in MeOH. Excess MeOH and water was removed in vacuum (10^{-4} mbar) for two days. Crystallization was induced by cooling to 280 K. XRPD analysis was not attempted owing to the deliquescence of the crystals.

2.2 Data collection and reduction

The crystals were immersed in perfluorinated polyether oil and quickly attached to Kapton micro mounts under a polarizing microscope. Mounting crystals of $TMA{\cdot}H_2PO_3{\cdot}H_2O$ posed a challenge, because the cubic crystals are optically isotropic at room temperature and possess an index of refraction close to that of the employed polyether. Thus, the crystals were cut with a knife into reasonable sized fragments without visual feedback and then moved out of the oil to assess their shape and size.

Intensity data were collected in a dry stream of nitrogen on a Bruker Kappa APEX II diffractometer system equipped with a CCD detector using graphite monochromatized sealed tube Mo$K\alpha$ radiation. Frame data were converted to intensity values using SAINT-Plus and a correction for absorption effects was applied using the multi-scan approach implemented in SADABS [2]. $MA{\cdot}H_2PO_3$ and $DMA{\cdot}H_2PO_3$ crystals were immersed directly into a 100 K N_2 stream. $TMA{\cdot}H_2PO_3{\cdot}H_2O$ crystals diffracted poorly when cooled quickly below phase transition temperature. Therefore, the $TMA{\cdot}H_2PO_3{\cdot}H_2O$ crystal described herein was mounted at 250 K and then measured at 200, 150 and 100 K with a cooling rate of 240 K/h before each measurement.

The structures were solved with SHELXT [3] and refined against F^2 using SHELXL [4]. H atoms attached to C were placed at calculated positions and refined as riding on their parent atoms. H atoms attached to P and N were refined freely and the P–H, N–H and O–H distances restrained to 1.350 (1) Å (P) and 0.870 (1) Å (N, O). The water and phosphonate O atoms in the HT structure of $TMA{\cdot}H_2PO_3{\cdot}H_2O$ were refined as positionally disordered about two positions. The total occupancy was constrained to 1 and the occupancy of both minor positions constrained to the same value. Likewise, a phosphonate O atom was refined as positionally disordered in $DMA{\cdot}H_2PO_3$, owing to a distinct peak in the difference Fourier map, which could not be explained by other means.

Since the low-temperature (LT) structure of $TMA{\cdot}H_2PO_3{\cdot}H_2O$ has orthorhombic $P2_12_12_1$ symmetry, the directions of three axes can in principle be chosen arbitrarily among the three directions of the 2_1screw axes. Formally, this is described by the affine normalizer [5] of $P2_12_12_1$, which contains affine transformations that permutate the axes. However, the conventional cell choice fixes the orientation of the basis according to the $a < b < c$ condition on the cell parameters, with the caveat that the b and c parameters are very close (ca. 9.61 vs. 9.63 Å or less than 0.2% difference) and their order might have been misdetermined owing to twinning. For consistency reasons, this setting was used for the LT phase.

In contrast, the high-temperature (HT) structure of $TMA{\cdot}H_2PO_3{\cdot}H_2O$ features the cubic $P2_13$ symmetry, which is devoid of the fourfold rotation of the cubic primitive (cP) lattice. Therefore, the structure can be described in two orientations, which are related by this fourfold rotation and the conventional cell choice does not give precedence over one of the two. In this case, the orientation was chosen in such a way that the coordinates of the HT phase are comparable to those of the LT phase. Thereto, the coordinate system had to be rotated by 90° about [100] with respect to the setting arbitrarily chosen by the diffractometer software.

More data collection and structure refinement data are collected in Table 1. Model data are deposited in the CIF format at the CCDC and can be retrieved using the deposition numbers listed at the bottom of Table 1.

3 Results and discussion

3.1 General remarks

The structures of the crystals under investigation follow the expected building mechanisms. The $H_2PO_3^-$ dihydrogen phosphite anions exist as the $HPO_2(OH)$ tautomer, i.e. one H is attached directly to P. The ion adopts a distorted trigonal pyramidal geometry with the P–O distance of the OH group significantly longer than of the other two O atoms (ca. 1.57 vs. 1.50 Å, see Table 2), which compares well to neutron diffraction derived data published by [6]. Note that the standard uncertainty on the P–O1 distance of $DMA{\cdot}H_2PO_3$ is distinctly larger owing to positional disorder of the O1 atom.

All structures are simple in the sense that the asymmetric unit contains at most one formula unit ($Z' = 1$). In the HT phase of $TMA{\cdot}H_2PO_3{\cdot}H_2O$, this number is even reduced to $Z' = \frac{1}{3}$. The structures are characterized by the maximization of hydrogen bonding, whereby the H atom attached to P does not partake in the hydrogen bonding. Indeed, with increased alkylation of the ammonium group (and thus less hydrogen bond donors), crystallization and handling owing to deliquescence became more difficult, with the trimethylammonium salt not crystallizing and the TMA salt crystallizing with water acting as hydrogen bond donor. All hydrogen bonds in the structures discussed herein are of moderate strength according to the classification of [7]; which means that their strength corresponds to the strength of hydrogen bonds of water at standard conditions.

Table 1: Data collection and structure refinement details.

	$MA{\cdot}H_2PO_3$	$DMA{\cdot}H_2PO_3$	$TMA{\cdot}H_2PO_3{\cdot}H_2O$	$TMA{\cdot}H_2PO_3{\cdot}H_2O$
Crystal data				
Chemical formula	CH_8NO_3P	$C_2H_{10}NO_3P$	$C_4H_{16}NO_4P$	$C_4H_{16}NO_4P$
M_r	113.05	127.08	173.15	173.15
Temperature (K)	100	100	100	150
Crystal system, space group	Monoclinic, $I2/a$	Monoclinic, $P2_1/c$	Orthorhombic, $P2_12_12_1$	Cubic, $P2_13$
a, b, c (Å)	8.2503 (5), 12.5988 (7), 9.6822 (5)	5.6086 (13), 11.554 (2), 9.544 (2)	9.4907 (18), 9.6078 (19), 9.6270 (18)	9.639 (2), 9.639 (2), 9.639 (2)
β (°)	93.252 (4)	96.556 (5)	90	90
V (Å^3)	1004.78 (10)	614.4 (2)	877.8 (3)	895.6 (6)
Z	8	4	4	4
Radiation type	Mo $K\alpha$	Mo $K\alpha$	Mo $K\alpha$	Mo $K\alpha$
μ (mm^{-1})	0.43	0.36	0.28	0.28
Crystal size (mm)	0.30 × 0.17 × 0.02	0.40 × 0.25 × 0.12	0.32 × 0.30 × 0.17	0.32 × 0.30 × 0.17
Data collection				
Diffractometer	Bruker Kappa Apex II CCD	Bruker Kappa Apex II CCD	Bruker Kappa Apex II CCD	Bruker Kappa Apex II CCD
Absorption correction	Multi-scan (Sadabs)	Multi-scan (Sadabs)	Multi-scan (Sadabs)	Multi-scan (Sadabs)
T_{min}, T_{max}	0.442, 0.497	0.220, 0.272	0.441, 0.493	0.441, 0.493
No. of measured, independent and observed [$I > 2\sigma(I)$] reflections	12364, 2252, 2024	9350, 2739, 2385	10019, 2478, 2360	9200, 870, 847
R_{int}	0.029	0.022	0.032	0.028
Refinement				
$(\sin\theta/\lambda)_{max}$ (Å^{-1})	0.811	0.815	0.706	0.704
$R[F^2 > 2\sigma(F^2)]$, $wR(F^2)$, S	0.022, 0.062, 1.06	0.025, 0.072, 1.06	0.038, 0.085, 1.24	0.021, 0.058, 1.08
No. of parameters	72	86	113	49
No. of restraints	5	4	4	4
$\Delta\rho_{max}$, $\Delta\rho_{min}$ (e Å^{-3})	0.57, −0.35	0.43, −0.32	0.54, −0.49	0.20, −0.11
Twin operations	–	–	$3^+_{[111]}$, $3^-_{[111]}$	–
Twin volume fractions	–	–	63.9:25.5:10.6 (8)	–
Flack parameter	–	–	−0.04(3)	−0.08(3)
CCDC number	2036785	2036786	2036787	2036788

Table 2: P–O distances in the crystals under investigation and LiH_2PO_3 [6]. The O atom of the hydrogen bond donating hydroxyl fragment is O3. The hydrogen bond acceptor of the hydoroxyl group is O2. The HT phase of $TMA{\cdot}H_2PO_3{\cdot}H_2O$ is not listed because the $H_2PO_3^-$ anion is disordered.

Crystal	P1–O1 (Å)	P1–O2 (Å)	P1–O3 (Å)
$MA{\cdot}H_2PO_3$	1.5041 (5)	1.5077 (5)	1.5743 (6)
$DMA{\cdot}H_2PO_3$	1.503 (2)	1.4999 (6)	1.5728 (6)
$TMA{\cdot}H_2PO_3{\cdot}H_2O$, 100 K	1.481 (4)	1.496 (4)	1.568 (4)
LiH_2PO_3	1.497 (2)	1.506 (2)	1.586 (2)

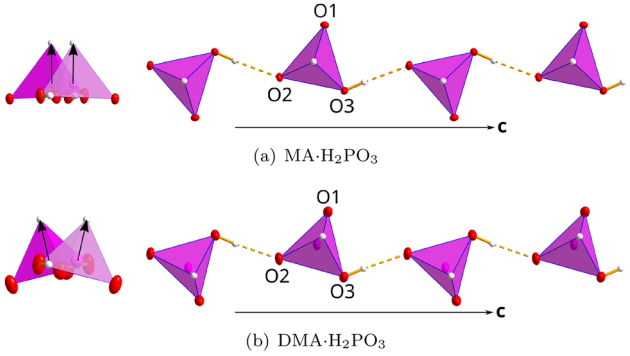

Figure 1: Chains of hydrogen bonded $H_2PO_3^-$ ions in (a) $MA{\cdot}H_2PO_3$ and (b) $DMA{\cdot}H_2PO_3$ extending along [100] viewed down [001] and [100] (left and right, respectively). P (pink), O (red) and C (gray) atoms are represented by ellipsoids drawn at the 50% probability levels, H atoms (white) by sphere of arbitrary radius. H···O hydrogen bonds are represented by dashed lines. In the [100] views, the direction of P–H-bonds are indicated by arrows. The minor (ca. 5%) positions of O1 in $DMA{\cdot}H_2PO_3$ are omitted for clarity.

3.2 $MA{\cdot}H_2PO_3$ and $DMA{\cdot}H_2PO_3$

The main building blocks of $MA{\cdot}H_2PO_3$ and $DMA{\cdot}H_2PO_3$ are infinite chains of $H_2PO_3^-$ ions connected by hydrogen bonding (Figure 1). In both cases, the chains are located

on glide reflection planes. The shapes of the chains are overall similar, with the H atoms attached to P pointing in the same direction. The precise conformation though is dictated by the hydrogen bonding from the MA and DMA cations. Whereas in MA·H_2PO_3 the P–H bonds are virtually parallel to the glide plane, they are distinctly inclined in DMA·H_2PO_3 (arrows in Figure 1, left).

Variations of such hydrogen-bonded chains of $H_2PO_3^-$ ions have been described for the non-hydrous salts LiH_2PO_3 [6], KH_2PO_3 [8] and $(NH_4)H_2PO_3$ [9]. In all cases, the chains are located on a glide reflection plane. However, in the K salt the chains are built of two crystallographically independent $H_2PO_3^-$ ions. Finite hydrogen bonding networks of $H_2PO_3^-$ ions have been observed in non-hydrous salts of di- and trivalent metals. Trimers are observed in $Fe(H_2PO_3)_3$ [10]; tetramers in $Cu(H_2PO_3)_2$ [11] and $Sr(H_2PO_3)_2$ [12].

In MA·H_2PO_3, the MA ion donates with all three ammonium H atoms to three distinct chains, thus forming a triperiodic network (Figure 2(a)). The DMA ion in DMA·H_2PO_3, on the other hand, possesses only two ammonium Hs, and each ion therefore connects only two chains, ultimately leading to a diperiodic hydrogen bonding network, which extends parallel to (100) (Figure 2(b)).

In DMA·H_2PO_3, the DMA ion donates only to the O atom of $H_2PO_3^-$ that is not involved in inner-chain hydrogen bonding (O1, see Figure 1). In MA·H_2PO_3, the MA ion additionally donates to the acceptor of the $H_2PO_3^-$ to $H_2PO_3^-$ hydrogen bond (O2). The trend is continued by the unsubstituted ammonium salt [9], where the NH_4^+ ion donates to all three atoms of the $H_2PO_3^-$ ion. The result is a distinctly more twisted chain of $H_2PO_3^-$ ions.

3.3 TMA·H_2PO_3·H_2O

3.3.1 HT phase

The HT phase of TMA·H_2PO_3·H_2O crystallizes in the cubic $P2_13$ symmetry. The TMA cation, the $H_2PO_3^-$ anion and the H_2O molecule are all located on the special position with threefold rotation symmetry. Note that all threefold rotation axes in $P2_13$ crystals are equivalent with respect to space group symmetry and they all belong to the unique special position.

Since the O atom of the water molecule is located (on average) on the threefold axis, it is formally connected to 3 H atoms, which therefore must feature an occupancy of $\frac{2}{3}$ to satisfy the H_2O stoichiometry. Likewise, since the HP fragment of the $H_2PO_3^-$ anion is located on the threefold axis, the hydroxyl H features an occupancy of $\frac{1}{3}$.

Thus, every H_2O molecule and every $H_2PO_3^-$ anion takes part in three disordered hydrogen bonds, whereby in two thirds of the cases H_2O acts as donor and in the remaining third $H_2PO_3^-$ is the donor. A given H_2O molecule thus switches between three states according to the scheme

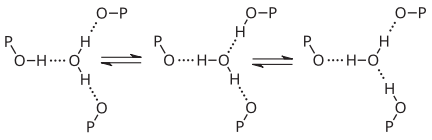

(2)

resulting on average in a site with 3 symmetry. The H_2O molecules on a threefold axis in the [111]direction connects to three $H_2PO_3^-$ anions on axes precisely in the three other directions $[\bar{1}11]$, $[1\bar{1}1]$, $[\bar{1}\bar{1}1]$. Note that in the $P2_13$ type of space group, these threefold rotation axes do not intersect, since such an

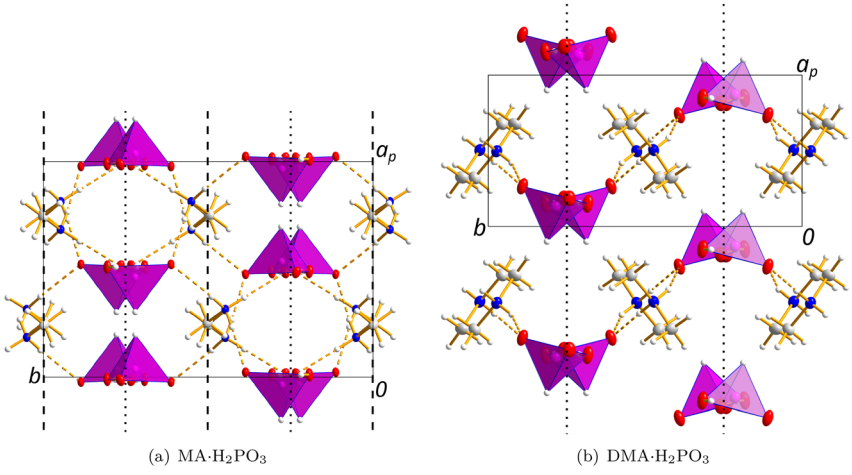

(a) MA·H_2PO_3 (b) DMA·H_2PO_3

Figure 2: The crystal structures of (a) MA·H_2PO_3 and (b) DMA·H_2PO_3 viewed down [001]. *a*- and *c*-glide planes are represented by the usual symbols, viz. dashed (intrinsic translation parallel to the drawing plane) and dotted (perpendicular to the drawing plane) lines, respectively. Atom color codes as in Figure 1, N atoms are blue.

intersection would correspond to a site with 23 symmetry, as it is found in the symmorphic *P*23 type of space group.

The situation is analogous for the $H_2PO_3^-$ anion, which switches between three states according to

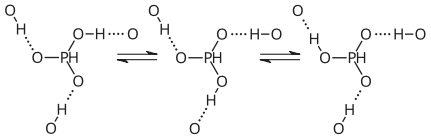

(3)

and likewise connects to H_2O molecules located on threefold axes in precisely the other directions.

Combining these fragments, a rather complex triperiodic hydrogen bonding network is formed. In the free space of this network are located the TMA anions, which do not partake in hydrogen bonding owing to a lack of donor and acceptor groups (Figure 3). The view down [111] shows the threefold symmetry.

The intricate triperiodic hydrogen bonding network can be conveniently represented using a labeled quotient graph [14], where every node represents an ion or molecule and all its translationally equivalents:

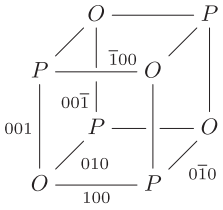

(4)

Here, *P* and *O* nodes stand for $H_2PO_3^-$ anions and H_2O molecules, respectively. Edges represent hydrogen bonds. A label (voltage) on an edge indicates that the representative H_2O molecule in the unit cell is connected to an $H_2PO_3^-$ ion outside the unit cell and the label describes in fractional coordinates the vector of the lattice translation that moves the $H_2PO_3^-$ ion into the unit cell. Note that all labels are to be interpreted for $O \rightarrow P$ steps. When moving in the opposite direction, the translation vector has to be inverted.

The graph above is arranged in the form of a cube to highlight the cubic 23 point symmetry: *P* and *O* nodes on the same space diagonal of the cube are located on threefold axes in the same direction in the actual structure. However, to trace paths in the graph, a planarized version such as

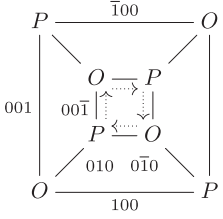

(5)

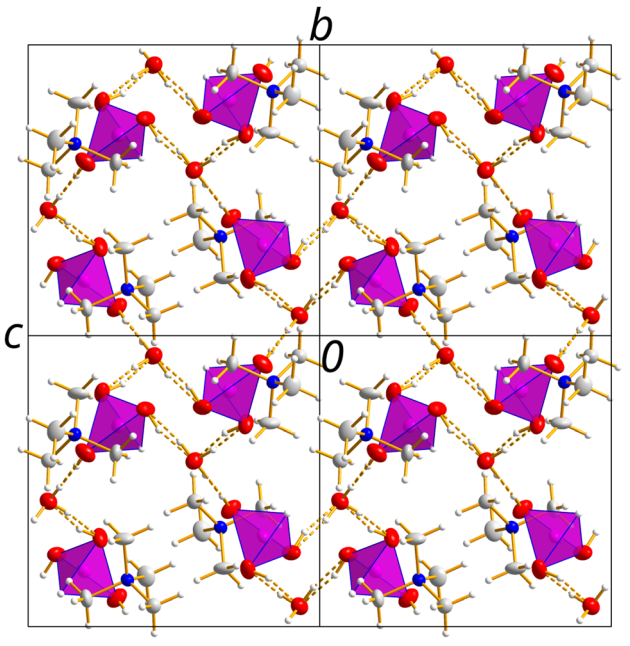

(a)

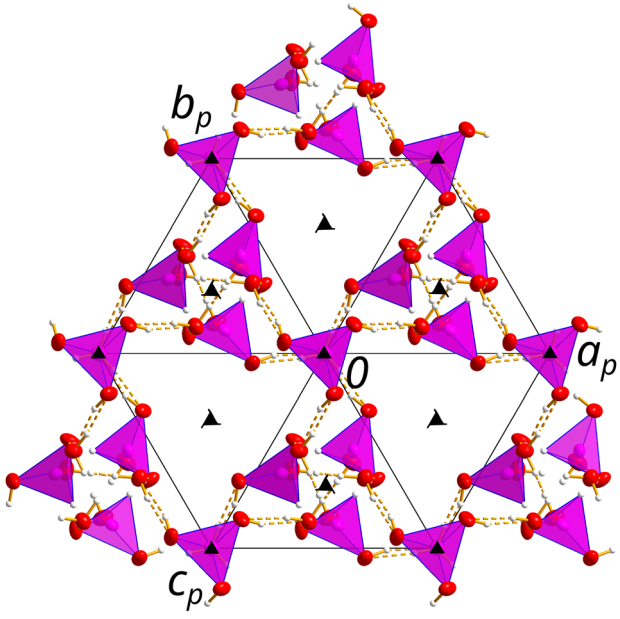

(b)

Figure 3: The cubic HT phase of TMA·H_2PO_3·H_2O viewed down (a) [100] and (b) [111]. Atom colors as in Figure 2. The TMA ions are omitted in (b) for clarity. Threefold rotation and screw rotation axes in (b) are are indicated by the usual symbols [13]. The minor positions of the O atoms (ca. 7%) are omitted for clarity.

is more convenient. The dotted arrows in Eq. (5) indicate the walk around a face of the "cube". However, such a cycle in the graph does not correspond to a cycle in the actual hydrogen bonding network. Indeed, summation of the voltages in the case above leads to a lattice translation in the

[001] direction for every full cycle. Thus, the indicated path corresponds to a helicoidal structure with period four (with respect to translational equivalence) about an 2_1 axis. These helices extend in the three main directions ⟨100⟩. An example of each direction is shown in Figure 4 by blue ([100]), green ([010]) and yellow ([001]) backdrops. Each direction corresponds to a pair of opposing faces in the "cube" and each face of such a pair corresponds to two opposite orientations of the chain.

The shortest actual cycle in the structure is obtained by combining two walks about two opposing faces of the "cube" as depicted in

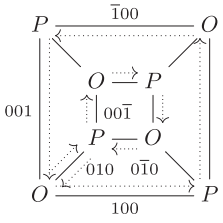

(6)

because paths on opposing faces screw in opposing directions. In this path, the sum of the voltages is the zero translation. Note that the edge that is crossed twice in the graph corresponds to two different bonds in the actual structure, which are related by a lattice translation. Such a ten-node cycle is highlighted by red color in Figure 4(b) and shown in Figure 5. The translationally equivalent $H_2PO_3^-$ ions and water molecules are connected by arrows.

In addition to the disordered hydrogen bonding, distinct electron density in the difference Fourier maps showed that the H_2O molecule features additional, most likely dynamical, disorder. Both positions are located on the three fold rotation axis. Refinement of the occupancies of both positions, while constraining the sum to 1 led to a 93:70 (5) ratio. The O atoms of the $H_2PO_3^-$ anions follow suit as shown in Figure 6 This minor positional disorder does not affect the overall hydrogen bonding network.

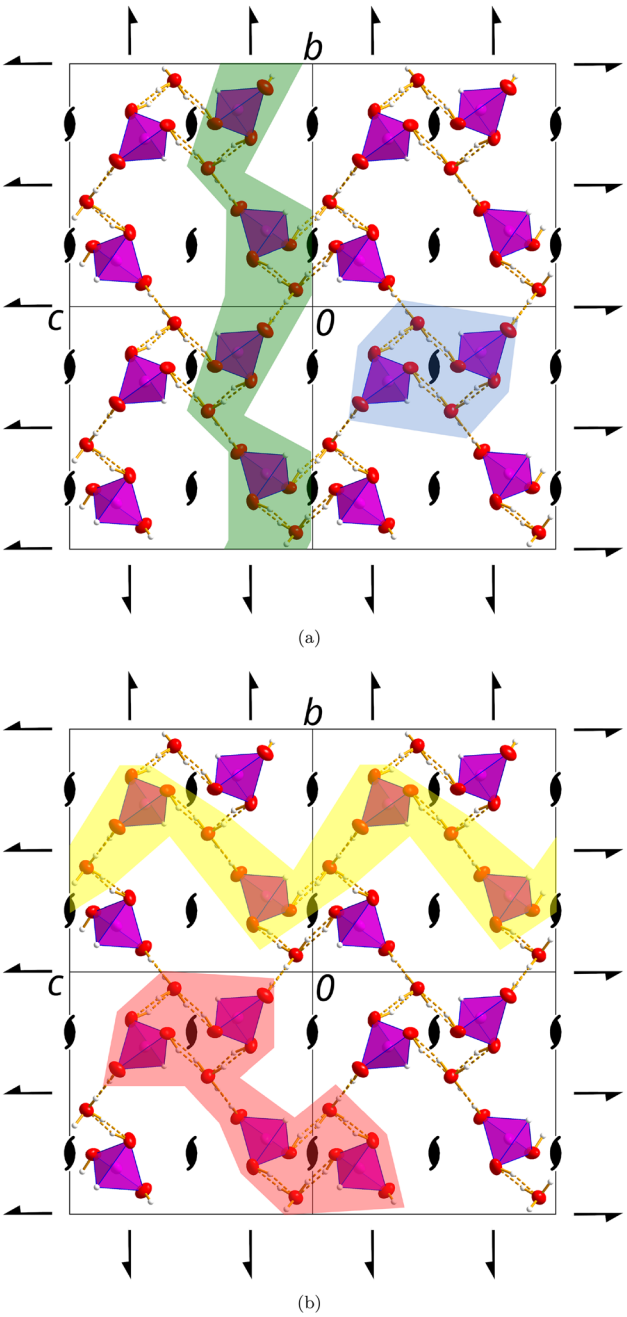

Figure 4: The HT phase of TMA·H_2PO_3·H_2O viewed down [100], with TMA ions omitted for clarity. The same projection is given twice to avoid overlap of the colored regions. Atom colors as in Figure 1. 2_1 screw rotations axes are indicated by the usual symbols [13]. Examples of helicoidal chains of the hydrogen-bonding network with two $H_2PO_3^-$ ions and two water molecules per translation period are highlighted by green, blue and yellow regions. An example of a ten-node cycle is highlighted in red. The minor positions of the O atoms (ca. 7%) are omitted for clarity.

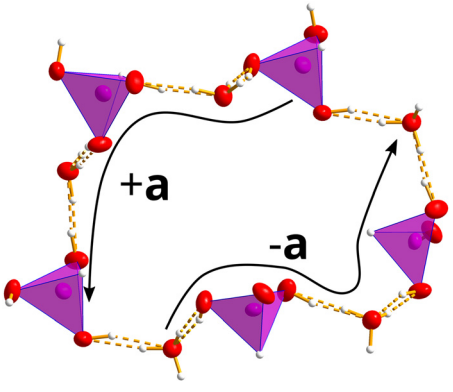

Figure 5: A ten-node cycle in TMA·H_2PO_3·H_2O. Atom colors as in Figure 1. The two four-node helix fragments (from H_2O to H_2O and from $H_2PO_3^-$ to $H_2PO_3^-$) are indicated by arrows, which are marked with the translations relating the two end groups.

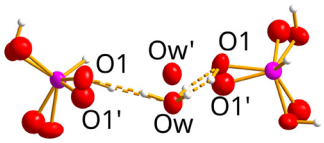

Figure 6: Disorder of a water molecule connecting two $H_2PO_3^-$ ions. The minor positions (ca. 7%) of the hydroxyl and water O atoms are labeled as O1′ and Ow′, respectively. Hydrogen bonding of the minor position is not shown, since the H atoms were not determined.

3.3.2 LT phase

On cooling, both disorders of the HT phase (hydrogen bonding network and positional disorder) are "frozen". The minor position of the positional disorder is never realized and for every $H_2PO_3^-$ ion and for every H_2O molecule in the crystal precisely one of the three states given in Eqs. (2) and (3) is realized.

Under the assumption that the LT phase is fully ordered, all threefold rotation axes are lost on cooling, because a threefold rotation is incompatible with the symmetry of H_2O and $H_2PO_3^-$. Thus, the symmetry of the LT phase cannot be cubic, as all cubic space groups feature threefold rotations. It could either be trigonal (via $P2_13 \rightarrow R3 \rightarrow P3_1/P3_2$), orthorhombic (via $P2_13 \rightarrow P2_12_12_1$) or of even lower symmetry. Note that the $P3_1/P3_2$ space groups possess only threefold screw rotations and such a structure could be ordered with respect to the hydrogen bonding. All trigonal space groups with a rhombohedral lattice, on the other hand, always contain threefold rotations and thus some disorder must still exist. However, experimentally a $P3_1/P3_2$ LT phase can be excluded, since the transition includes a symmetry descent of the *klassengleiche* type ($R3 \rightarrow P3_1/P3_2$). This corresponds to a reduction of translation symmetry and therefore appearance of superstructure reflections. However, no reflections compatible with such a hexagonal primitive (*hP*) lattice were observed.

A priori, we can of course not rule out that the LT phase is partially disordered and thus still features threefold rotations. The observed lattice is in principle compatible with *R*3 symmetry with with cell parameters analogous to the HT phase. However, overall the diffraction data was more consistent with an ordered orthorhombic $P2_12_12_1$ structure than any other model. The point symmetry of the intensity data was more in line with an orthorhombic than a rhombohedral space group (R_{int} = 2.8% for $P2_12_12_1$ vs. R_{int} > 10% for *R*3). Moreover, a very convincing model was obtained in the $P2_12_12_1$ space group, featuring no disorder and the expected geometry of the ordered $H_2PO_3^-$ anion, with one distinctly longer P–O-bond (see Table 2). This model refined to lower residuals than *R*3 models. For the latter, even when modeling as a fourfold twin by fourfold rotation about [100], $R[F^2 > 2\sigma(F^2)]$ could not be brought below 7%, in contrast to 3.8% for the $P2_12_12_1$ model presented here.

The $P2_12_12_1$ space group has no special positions, thus the symmetries of the TMA cation, the $H_2PO_3^-$ anion and the H_2O molecule are decreased from 3 to 1. On the atomic level, as expected in a symmetry reduction, the atomic positions are split and/or the occupancies are increased [15], as summarized in Table 3. The H atoms of the water molecule feature both phenomena, namely the single HT position is split in two LT positions *and* the occupancy is increased from $\frac{2}{3}$ to 1.

Since the hydrogen bonding is ordered in the LT phase, it can be represented by the directed graph

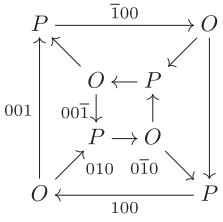

(7)

where an → arrow indicates a directed O–H···O bond. Accordingly, every *O* (H_2O) node has two outgoing and one incoming edge and vice-versa for *P* ($H_2PO_3^-$) nodes. Again, the given voltages are to be read in the $O \rightarrow P$ direction and independent of the direction of the edges. From the graph one can immediately see the loss of the threefold rotations and therefore cubic symmetry. Moreover by tracing paths

Table 3: Site symmetry group and occupancy of atoms in the HT and LT phases of TMA·H_2PO_3·H_2O. Methyl Hs are not listed and positional disorder of the O atoms is ignored. Ow designates the water molecule, other O atoms belong to the $H_2PO_3^-$ anion.

LT			HT		
Atom	**Site symmetry group**	**Occ.**	**Atom**	**Site symmetry group**	**Occ.**
P1	3	1	P1	1	1
Hp1	3	1	Hp1	1	1
O1	1	1	O1	1	1
			O2	1	1
			O3	1	1
Ho1	1	$\frac{1}{3}$	Ho3	1	1
Ow	3	1	Ow	1	1
Hw1	1	$\frac{2}{3}$	Hw1	1	1
			Hw2	1	1
N1	3	1	N1	1	1
C1	3	1	C1	1	1
C2	1	1	C2	1	1
			C3	1	1
			C4	1	1

along the faces of the "cube", one can see that by following hydrogen bonds in the donor → acceptor direction the helicoidal structures with 2_1 symmetry are retained in the [100], [$\bar{1}$00], [001] and [00$\bar{1}$] directions (Figure 7). In the [010] and [0$\bar{1}$0] directions, on the other hand, hydrogen bonds have to be crossed in two different directions (green region in Figure 7).

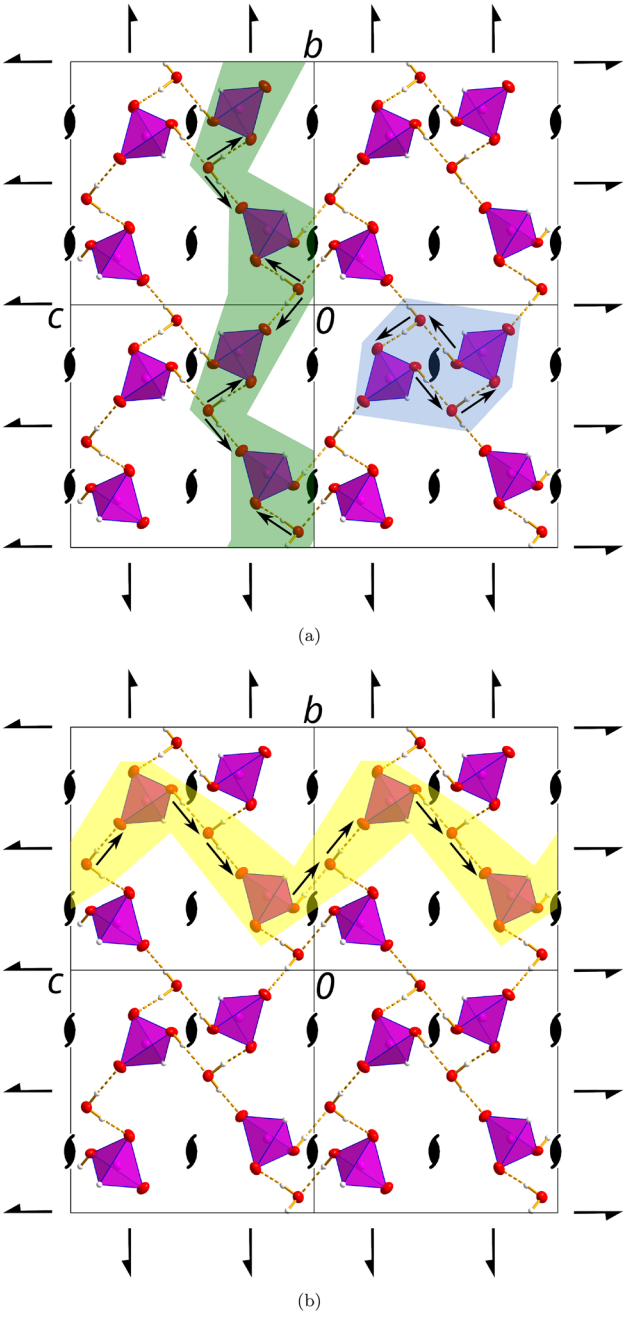

Figure 7: Hydrogen bonding network in the LT phase of TMA·H_2PO_3·H_2O viewed down [100]. Color codes of atoms and helices as in Figure 4. Directed hydrogen bonds in the highlighted areas are indicated by arrows.

3.3.3 Twinning

The cubic 23 point group of the HT phase is a merohedry, which means that it is of a lower symmetry than the $m\bar{3}m$ point group of the cubic lattice. More precisely, it is a tetartohedry, i.e. the index of 23 in $m\bar{3}m$ is $|m\bar{3}m| : |23| = 4$. For a given cubic lattice, the structure can therefore appear in four orientations, which are derived by coset decomposition of 23 in $m\bar{3}m$. In principle, crystalline domains of these orientations could be present in the same sample, which would then be a twin by merohedry [16]. However, in all experiments we could exclude twinning by fourfold rotation about ⟨100⟩ or by the corresponding fourfold rotoinversion. For the HT data set discussed here, the twin volume ratio of such a putative twin domain refined to −0.002 (6), i.e. to zero within the experimental error. Likewise, we did not find hints of twinning by inversion, though here the experimental uncertainty is larger by a factor of 5, since even the heaviest atom in the structure (P) is not a significant anomalous scatterer under the employed Mo *Kα* radiation [Flack parameter −0.04 (3)]. In summary, the TMA·H_2PO_3·H_2O crystals are generally not twinned above the phase transition temperature.

For twinning to occur, there needs to be a continuity of either an arbitrary substructure [17] or in the form of full layers as in the order-disorder (OD) theory [18], which apparently is not the case here. Note that the OD theory is unrelated to the order-disorder type of phase transition described herein.

The 222 point group of the LT phase is a subgroup of index $|23| : |222| = 3$ with respect to the 23 point group of the HT phase. Thus, on cooling of the HT phase, one can expect formation of threefold twins. Indeed, we invariably observed splitting of reflections in agreement with threefold twinning when measuring TMA·H_2PO_3·H_2O at low temperatures. The twin laws are derived by coset decomposition of 222 in 23. The second and third orientation are related to the first by the representative $3^+_{[111]}$ and $3^-_{[111]}$ operations, respectively. The remaining operations of the twin laws are threefold rotations about the other space diagonals, [$\bar{1}$11], [1$\bar{1}$1] and [11$\bar{1}$]. The symmetry of the threefold twin is conveniently represented by the trichromatic point group $(23^{(3)})^{(3)}$ [19]. This symbol indicates that the overall point symmetry of the twin is of type 23, whereby the 3 operations are trichromatic (interchanges domains in cycles of size 3) and the 2 operations are achromatic, as they are point operations of all three twin domains.

Since the translation lattice remains in principle unchanged during the phase transition (neglecting the small

deviation from cubic metrics), the twinning is by *pseudo-merohedry*. This means that the twin index is $n = 1$, i.e. all three twin individuals possess diffraction spots at (approximately) the same location in reciprocal space. The deviation from cubic metrics causes a splitting of reflections, which is expressed by the twin obliquity ω, the angle of the three-fold [111] rotation axis to the normal of the (111) plane. For the orthorhombic lattice of the LT phase of $TMA{\cdot}H_2PO_3{\cdot}H_2O$ it calculates as

$$\omega = \cos^{-1}\left(\frac{3}{\sqrt{\left(\frac{1}{a^2}+\frac{1}{b^2}+\frac{1}{c^2}\right)(a^2+b^2+c^2)}}\right) \qquad (8)$$

which, using the cell parameters of the LT phase, gives $\omega \approx 0.70°$. However, this estimate is certainly smaller than the actual twin obliquity, because integration of frame data was performed using a single domain, which therefore represents an average of the three domains. To determine more reliable cell parameters, and thus a more precise twin obliquity, high-resolution (powder) diffraction would be needed.

3.4 Conclusion and outlook

The structure of $TMA{\cdot}H_2PO_3{\cdot}H_2O$ is seemingly trivial with only one third (HT) or one (LT) formula unit in the asymmetric unit. Nevertheless, owing to the cubic symmetry a surprisingly intricate hydrogen bonding network is formed. An analysis of the hydrogen-bonding topology and the symmetry relations clears the fog and simplifies these complexities, which arise from simple building principles. Tracing paths in a planarized voltage graph significantly facilitates the identification of infinite motifs in a triperiodic network. Moreover, in this case, the order-disorder phase transition can be represented by mapping directed and undirected graphs.

In general, for unsubstituted and methyl-substituted ammonium salts of dihydrogenphosphite the readiness to crystallize decreases with the number of hydrogens in the ammonium cation, showing the significance of hydrogen bonding in this system. In contradiction to this trend, we couldn't crystallize the trimethylammonium salt, whereas TMA crystallized inside an extended hydrogen bonding network formed by water and $H_2PO_3^-$. Interestingly, the exactly same behavior was observed for the hypophosphite ($HP^{I}O_2^-$) salts. The ammonium, MA and DMA salts crystallize readily. However, we could not crystallize any trimethylammonium salt, and yet TMA crystallized as a hydrate. This similarity of the behavior does not extend to the structures themselves, which are unrelated to the dihydrogenphosphites described herein, and will be presented elsewhere.

Acknowledgments: The constructive feedback of two anonymous referees is highly appreciated and distinctly improved the manuscript.
Author contributions: All the authors have accepted responsibility for the entire content of this submitted manuscript and approved submission.
Research funding: None declared.
Conflict of interest statement: The authors declare no conflicts of interest regarding this article.

References

1. Schmidt V. H. *Ferroelectrics* 1987, *72*, 157.
2. Bruker AXS Inc. *Apexii, Saint and Sadabs*: Madison, Wisconsin, USA, 2020.
3. Sheldrick G. M. *Acta Crystallogr. A* 2015, *71*, 3.
4. Sheldrick G. M. *Acta Crystallogr. C* 2015, *71*, 3.
5. Koch E., Fischer W., Müller U., Aroyo M. I. Normalizers of space groups and their use in crystallography. In *International Tables for Crystallography*; IUCr: Chester, Vol. *A*, 2016; p. 826.
6. Johansson G. B., Lindqvist O. *Acta Crystallogr. B* 1976, *32*, 412.
7. Jeffrey G. A. *An Introduction to Hydrogen Bonding*; Oxford University Press: Oxford, 1997.
8. Kratotochvíl B., Podlahová J., Hašek K. *Acta Crystallogr. C* 1983, *39*, 326.
9. Melichar Z., Kratochvíl B., Podlahová J., Petříček V., Malý K., Císařová I. *Acta Crystallogr. C* 1984, *40*, 720.
10. Sghyar M., Durand J., Cot L., Rafiq M. *Acta Crystallogr. C* 1991, *47*, 8.
11. Sghyar M., Durand J., Cot L., Rafiq M. *Acta Crystallogr. C* 1990, *46*, 1378.
12. Ouarsal R., Tahiri A. A., Bali B. E., Lachkar M., Bolte M. *Acta Crystallogr. E* 2002, *58*, i19.
13. Hahn Th., Aroyo M. I. Space-group symmetry. In Aroyo M. I., Ed. *International Tables for Crystallography*; IUCr: Chester, Vol. *A*, 2016; p. 144.
14. Eon J.-G. *Acta Crystallogr. A* 2011, *67*, 68.
15. Müller U. *Z. Anorg. Allg. Chem.* 2004, *630*, 1519.
16. Grimmer H., Nespolo M. *Z. Kristallogr.* 2006, *221*, 28.
17. Nespolo M., Souvignier B. *Cryst. Res. Technol.* 2015, *50*, 442.
18. Dornberger-Schiff K., Grell-Niemann H. *Acta Crystallogr.* 1961, *14*, 167.
19. Nespolo M. *Z. Kristallogr.* 2004, *219*, 57.